Additive-free electroless deposition on graphene/copper foil: Photo-induced and defect-assisted approach for environmentally friendly plating

Hsiao-Chien Chen [a,b,c,*], Abdul Shabir [a,d], Kun-Hua Tu [b], Cher Ming Tan [a,d,e,f,*], Wei-Hao Chiu [a], Ruei-Cheng Fan [a,d], Nilim Akash Baruah [a,d]

[a] Center for Reliability Science and Technologies, Chang Gung University, Taoyuan 33302, Taiwan
[b] Kidney Research Center, Department of Nephrology, Chang Gung Memorial Hospital, Linkou, Taoyuan 33305, Taiwan
[c] Center for Sustainability and Energy Tecnhologies, Chang Gung University, Taoyuan 33302, Taiwan
[d] Department of Electronic Engineering, College of Engineering, Chang Gung University, Taoyuan 33302, Taiwan
[e] Department of Radiation Oncology, Chang Gung Memorial Hospital, Taoyuan 33305, Taiwan
[f] Center for Reliability Engineering, Ming Chi University of Technology, New Taipei City 243303, Taiwan

ARTICLE INFO

ABSTRACT

The environmental toxicity of chemicals used in electroless plating process is often overlooked. In fact, the wastewater from the electroless plating process contains metal complexes, reducing agents and stabilizers that can create hazard to our environment. To address this concern, an additive-free electroless deposition process on graphene/Cu foil is proposed. The defect structure of graphene plays a pivotal role by acting as a reservoir for concentrating photoelectrons generated from ultra-thin cuprous oxide (Cu_2O) located at the interface of graphene and Cu foil upon exposure to light irradiation. In the Cu ion solution, Cu ions were anchored on the defect sites and formed a $Cu-C_4$ structure with graphene. The $Cu-C_4$ sites accumulate abundant photoelectrons and trigger the reduction of Cu ions to form island-like growth of Cu, which immediately was oxidized to Cu_2O, leaving only a small portion of metallic Cu. Concurrently, the presence of Cu ions induces the generation of additional defect sites on graphene, providing further growth sites for Cu deposition. This process continues until the entire graphene surface is covered by the deposited Cu_2O. Ultimately, the deposition of metallic oxides with lower redox potential can be achieved. The proposed deposition mechanism assisted by irradiation of photocatalyst and defect structure of graphene material provides a truly environmentally friendly electroless plating process. By eliminating the need for additives and significantly reducing the environmental hazards associated with electroless plating, this method holds great promise for sustainable materials manufacturing.

1. Introduction

Pollutants such as sludge waste baths and wastewater from the electroplating industry are invariably hazardous [1]. On the contrary, electroless plating process, also known as autocatalytic plating, which utilizes its self-catalysis property to induce a controllable redox reaction without applying electric power is considered environmentally friendly [2,3]. The minimum composition of an electroless plating bath consists of metal ions and reducing agents at a specific pH value. However, additives such as stabilizers, complexing agents and buffers are commonly added to electroless plating bath, resulting in a large amount of metal-organic compounds and chemical reagents in wastewater [4], which increases the cost of chemicals, wastewater management and environmental pollution risks. Therefore, reducing the amount and type of chemical reagents used is a prerequisite for the development of a truly green electroless plating process.

Recently, the approach of substrate-enhanced electroless deposition has attracted much attention because it does not involve reducing agents [5–7]. Meanwhile, the defect structures of carbon materials could provide anchor sites for metal atom via the strong charge transfer by 2π antibonding state of the carbon atoms for stabilizing metal atom [8]. These obtained single-atom metal atom/carbon materials exhibit high activity in catalytic reactions [6,9]. Additionally, the formation of metallic clusters and nanoparticles could be obtained for some noble

---

metals due to their higher redox potential [10,11]. Also, the defect structures possess lower work function than defect-free carbon structure, allowing noble metals to be preferentially deposited on the defect structure. However, the distribution of deposited metallic clusters and nanoparticles on the surface of carbon materials is dominated by the degree of defect structure. It means that the electroless deposition of uniform metallic layer cannot be achieved, especially for metal species with lower redox potentials, limiting its practical applications.

Recently, the deposition of cuprous oxide (Cu_2O) with lower redox potential on carbon materials has been of intense interest in photothermal conversion, antibacterial protection and photo/electrochemical catalytic reaction [12–16]. In particular, oxide-derived Cu is recognized as the most important catalysts toward electrochemical CO_2 reduction reaction since only Cu-based catalysts can effectively convert CO_2 into valuable hydrocarbon and alcohol products [17–20]. Meanwhile, carbon materials with large specific surface area and high conductivity endow synergistic activity with catalysts. The common method for coating the prepared Cu_2O onto carbon-based materials involves spraying a Cu_2O suspension. However, due to the weak interaction between Cu_2O and the substrate, it is prone to detachment, especially during electrochemical gas evolution reactions. To enhance the adhesion between Cu_2O particles and between Cu_2O and the substrate, a small amount of polymer, such as Nafion, is typically added to the Cu_2O solution [21,22]. Even more concerning is the use of various chemical reagents during the synthesis of Cu_2O nanoparticles. These reagents include stabilizers (polyethylene glycol or polyvinylpyrrolidone), reducing agents (ascorbic acid, sodium borohydride, polyvinylpyrrolidone or glucose), pH adjusters (sodium hydroxide or potassium hydroxide) and solvents (diethylene glycol or ethylene glycol)

[23–29]. The use of these chemicals not only increases production and subsequent treatment costs but also poses direct and potential risks to the environment when handled improperly.

In this work, an additive-free electroless deposition of Cu_2O on commercial graphene/Cu foil with the interface of Cu_2O is proposed by a photo-assisted process. We leverage on the photoelectric properties of Cu_2O to provide photoexcited electrons upon light irradiation, which are accumulated at the defect sites of graphene. The electron-rich sites serve to reduce Cu ions as well as to avoid the re-dissolution of deposited Cu_2O [30,31], in which the growth site started from the Cu-C bond at the defect structure. Simultaneously, the Cu ions in $CuSO_4$ solution induced the formation of defect structure as growth sites, which extend the deposition reaction to the entire graphene surface and achieve high-density deposition. Based on the evidences of in situ Raman spectroscopy, ex situ X-ray photoelectron spectroscopy (XPS) and X-ray absorption spectroscopy (XAS), the mechanism of electroless process on graphene/Cu foil surface is clarified.

2. Results and discussion

Fig. 1a showed the photo image of graphene/Cu foil obtained from Graphenea Inc. The growth method of graphene on Cu foil was adopted via chemical vapor deposition. The Raman spectrum shows two main peaks at 1589 and 2644 cm^{-1}, which are the assigned G band and 2D band (Fig. 1b). The number of graphene layer could be derived from the ratio of 2D to G band intensity. The value of I_{2D}/I_G is around 2, meaning the graphene on Cu foil is single layer graphene. A relatively weak D band from disordered graphite appearing at 1324 cm^{-1}, indicating a slight defect structure in graphene.
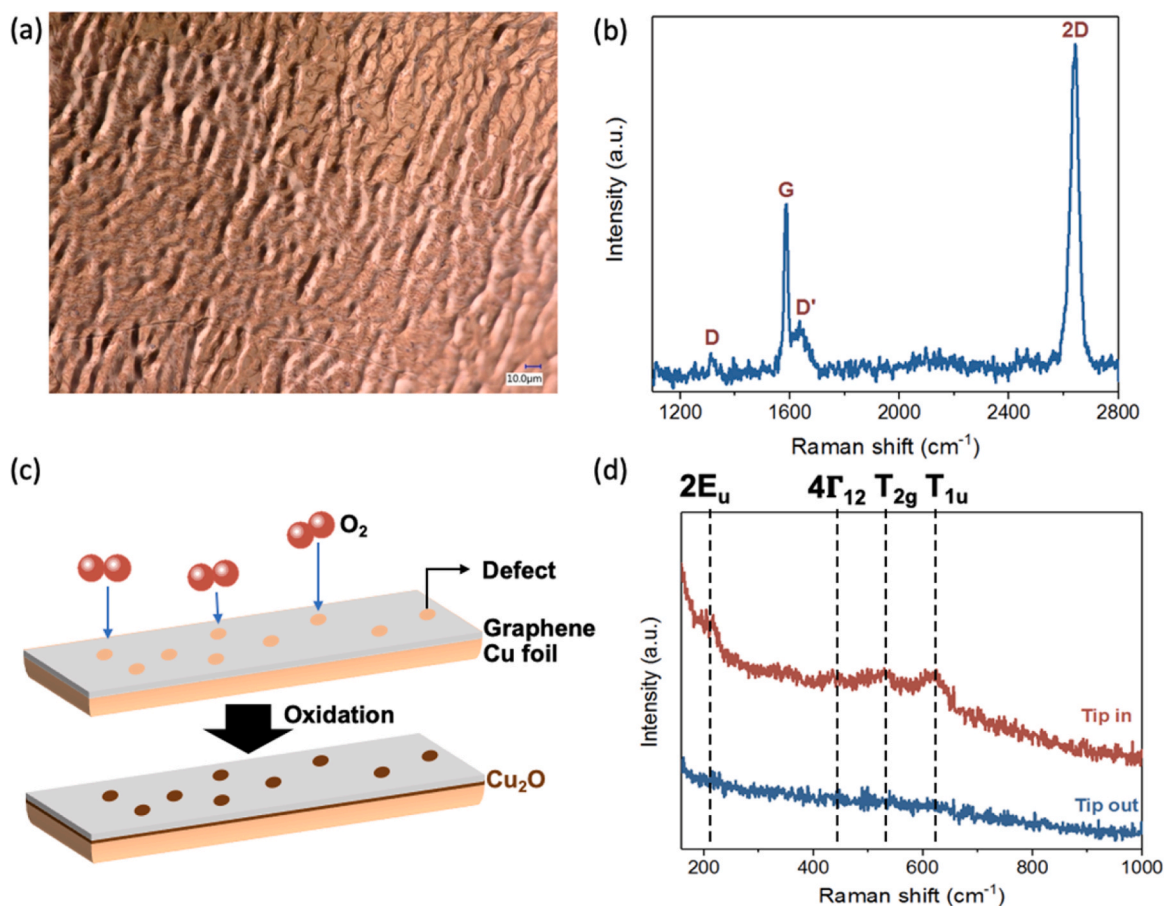
Fig. 1. (a) photo image of graphene/Cu foil. (b) Raman spectrum of graphene. (c) Scheme of Cu foil oxidation by the oxygen passing through the defect structure of single layer graphene. (d) The characteristic of the interface of graphene and Cu foil by TERS.

Literatures reported that the few-layer graphene on Cu surface would block the penetration channel of oxygen and water vapor reaching Cu surface, thus exhibiting the function of anticorrosion [32]. However, single-layer graphene structure containing a small number of defect sites can become a channel for oxygen to pass through, thereby oxidizing the surface of the Cu foil (Fig. 1c) [32]. It is worth noting that the small amount of defect structure presented in single-layer graphene that causes slight oxidation of Cu will be undetectable by conventional Raman spectroscopy without auxiliary enhancement methodology. By introducing the technique of tip-enhanced Raman spectroscopy (TERS) (Fig. 1d), some characteristic peaks of Cu_2O were observed at 211, 428, 523 and 621 cm^{-1} [33], indicating that a very thin Cu_2O film was indeed formed at the interface of graphene and Cu foil.

To clarify the structural state of graphene on Cu_2O surface, atomistic scale modelling and density functional theory calculations were employed to investigate the penetration of oxygen atoms from the slightly oxidized Cu layer through the defect channels of single layer graphene as shown in Fig. 1c. We modelled a system of a pristine copper block and layered it with 8 Cu_2O molecules. However, the interactions or bond formations was not pre-determined as shown in Fig. 2a and 2b. The combination of pristine Cu+Cu_2O molecules were geometrically optimized to attain a lower energy state using Vienna Ab-initio Simulation Package (VASP). After the geometry optimization, it is found that the Cu_2O molecules readily bonded with the pristine Cu system which resembles to a slightly oxidized Cu foil as mentioned earlier (Fig. 2b).

Subsequently, addition of a single layer of defective graphene is done and again the system is geometrically optimized. It is found that the presence of a single layer of defective graphene above the slightly oxidized Cu system upset the stability of the Cu system (Fig. 2c) in the following. Firstly, the oxygen atoms from the Cu_2O molecules slightly permeates through the defect channels of the graphene layer as shown in the green circles in Fig. 2d. Secondly, some Cu atoms dissociate the Cu-Cu bonding and form unstable bonds with the defect sites in the graphene layer as shown in the blue circles in the same Figure. As these reactions of the Cu-Cu_2O-graphene system occurs in a stable energy state (i.e. the structure is geometrically optimized for stability), they can potentially oxidize further in presence of suitable external energy.

The co-existence of defect structures of graphene and Cu_2O on the Cu foil surface provided a potential for electroless Cu plating on graphene. The defect structures act as reducing agents due to their lower work function and anchoring points for in situ growing metal cluster [10,34]. As investigated by density functional theory calculations, the binding energy of metallic atom to the defect site of graphene was higher than that of metallic atom-metallic atom and metallic atom-C (without defect structure) [7,35]. For instance, the Pt, Pd, Sn and Au atoms exhibit the binding energies of 7.234 eV, 5.237 eV, 4.487 eV and 2.345 eV to defect sites of graphene, which are higher than those binding energies of 1.552 eV, 1.077 eV, 0.200 eV and 0.075 eV to graphene without defect
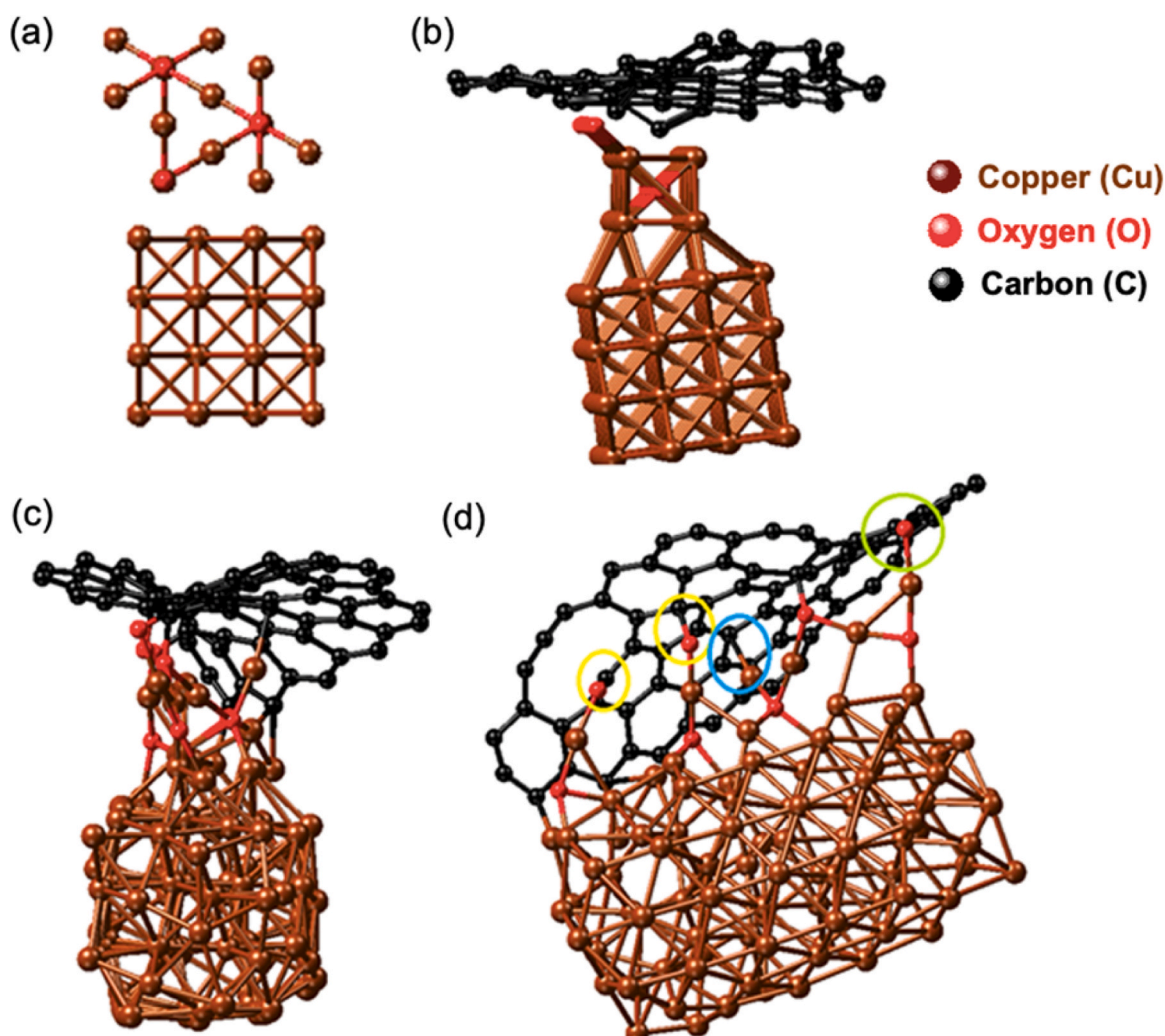
Fig. 2. (a) Cu and Cu_2O system modelling (b) Geometrically optimized Cu and Cu_2O system with single layer defective graphene (c) Complete geometrically optimized Cu and Cu_2O system with a single layer defective graphene (d) Green circle show oxygen atoms permeating through defect sites of graphene, blue circle show the bond formation between Cu and defect sites in the graphene and yellow circles show bond formation between O and defect sites in the graphene.

sites. Consequently, the metal clusters would generate with the additional metallic atoms received by the C sp^2-orbitals surrounding the defect sites. So far, only the Pt, Au and Pd clusters anchoring on the defect site were observed due to their higher redox potentials which were 1.19 V, 1.50 V and 0.92 V, respectively [29]. Additionally, the entire substrate was not completely covered by reduced metal because the presence of the reduction sites limited the extensive growth of metallic clusters [10]. However, electroless Cu plating on graphene via the above process was not achieve due to the relative lower redox potential at 0.34 V [36].

Now the existence of Cu$_2$O at the interface of graphene and Cu foil as observed could provide light-induced photoelectrons which can be further captured and concentrated at the defect sites. This phenomenon would enhance the reducing capacity and be able to assist the non-spontaneous reduction of Cu ion on the graphene surface. For the graphene/Cu foil, the interface of Cu$_2$O shows a wide absorption range in UV-Vis spectrum from 400 to 600 nm (Fig. 3a), which is close to that of Cu$_2$O nanoparticles and electrochemically deposited Cu$_2$O thin films [37,38]. This observation suggests the presence of Cu$_2$O at the interface between graphene and Cu, which had been confirmed by TERS (Fig. 1d). Besides, it also implies that photoelectrons can be induced when exposed to light of appropriate wavelength.

To study the feasibility of the above-mentioned, namely electroless Cu plating on graphene via light excitation, LEDs with various wavelength of emission light are used to generate different levels of photoexcited electrons. The PL spectra of the emission sources exhibit blue, green, red and white with the maximum wavelength of 463, 524, 632 and 452 coupling 547 nm, respectively. The experimental setups are shown in Fig. 3b and 3c, in which 1 cm^2 of graphene/Cu foils are respectively immersed in 5 mM of CuSO$_4$ with different irradiation wavelengths under constant stirring at 200 rpm.

Fig. 4 shows the time-dependent microscopic images of graphene/Cu foil surfaces in 5 mM of CuSO$_4$ solution at different emission wavelengths. Comparison of the images from 10 min to 4 h in the dark state show no reduction of Cu ions occurred due to the low reduction ability of

graphene defect structure without any assistance, and this could be the reason of no experimental evidence of spontaneous reduction of Cu on defect structure. Under the auxiliary irradiation of blue, green, red or white light LEDs whose emission wavelength satisfies the absorption of Cu$_2$O, obvious particles appear on the surface within 1 h, suggesting the generated photoexcited electrons endowed the graphene defect structure with stronger reduction ability. Upon prolonged light irradiation, more particles produced and grown until they were connected to each other and cover the entire surface of the graphene. In fact, some fine particles can be clearly observed after 10 min of green light irradiation, and the particle dispersion density was the highest. Furthermore, the 3D image of optical microscopy showed that the particles are actually formed, instead of being etched on the graphene/Cu foil (Fig. S1). Our results indicated the optimal light source is green light. This is expected because the maximum absorption of Cu$_2$O film from the interface of graphene/Cu foil was closed to 524 nm as shown in Fig. 3(a). The photo and scanning electron microscope (SEM) images further indicated the reduction and deposition keep happening at the particles edges, resulting in an increase in size over time (Fig. S2).

To identify the elements of the formed particles, EDS mapping is adopted to probe the element distribution. The elements of the generated particles include the Cu element as well as the oxygen element, suggesting the particles could be in oxidized state (Fig. S3). The in situ Raman spectroscopy with excitation wavelength of 532 nm shows the formation of Cu$_2$O with the characteristic peaks at 523 and 621 cm^{-1} in less than 5 mins (Fig. 5). Also, the intensity increased with immersion time, meaning that increasing amount of Cu$_2$O is produced. Besides, the XRD pattern shows the diffraction peaks at 29.6°, 36.7°, 42.6° and 61.7°, which were assigned to Cu$_2$O (JCPDS NO. 78–2076), revealing that the structure of the electroless Cu is Cu$_2$O, naming EL-Cu$_2$O (Fig. 5b).

Notably, the deposited Cu$_2$O could further provide the photoelectrons under exciting irradiation when the initial Cu$_2$O layer under the graphene is covered by the deposited particles, and thus assist the continuous growth of deposition over the surface of the samples (Fig. S4). This phenomenon was consistent to the observations from the
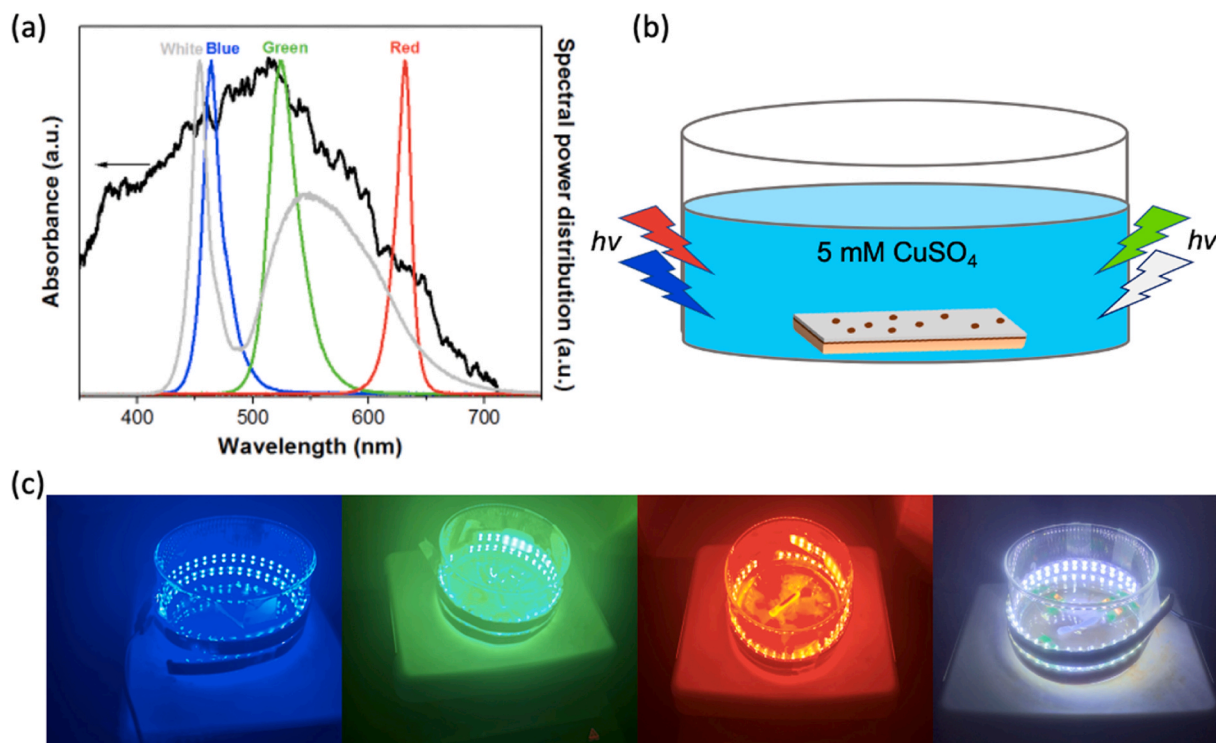
Fig. 3. (a) The absorption spectrum of graphene/Cu foil (black line) and the wavelength of emission of blue (blue line), green (green line), red (red line) and white (gray line) light LEDs. (b) Schematic and (c) photo images of the experimental setups for electroless Cu plating.
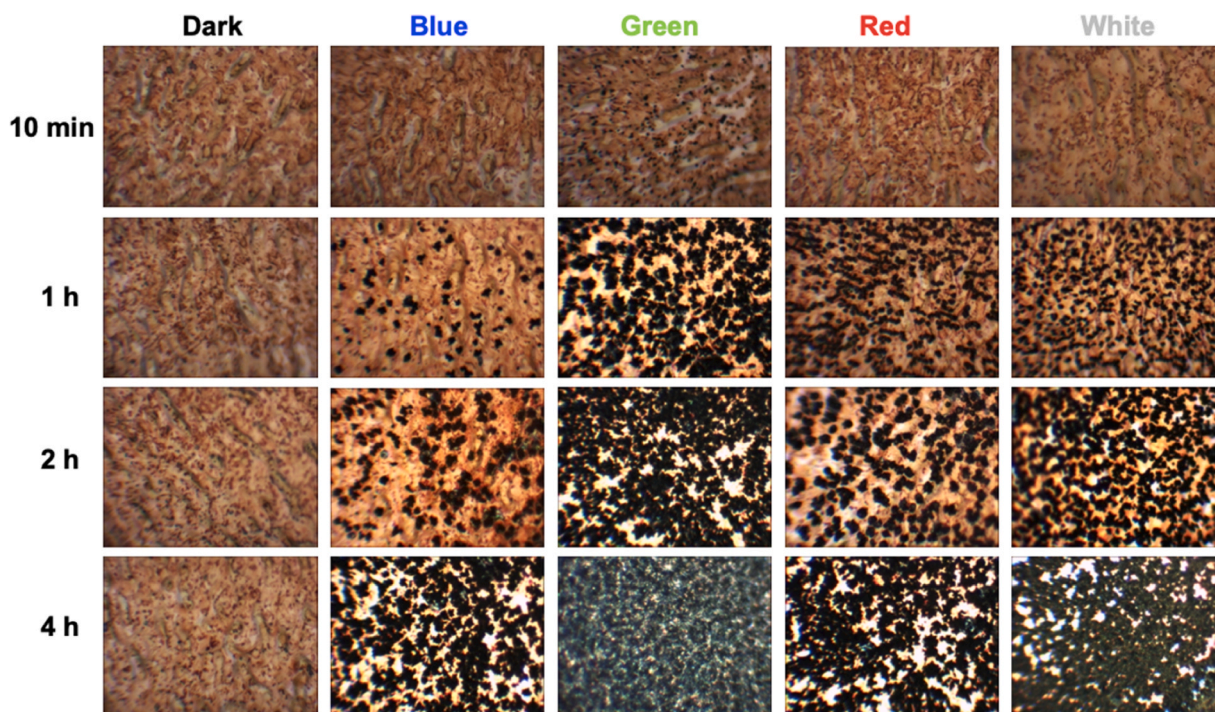
Fig. 4. Microscopy images (100 μm × 100 μm) of graphene/Cu foil surface in CuSO$_4$ solution at different time under various wavelength of emission.
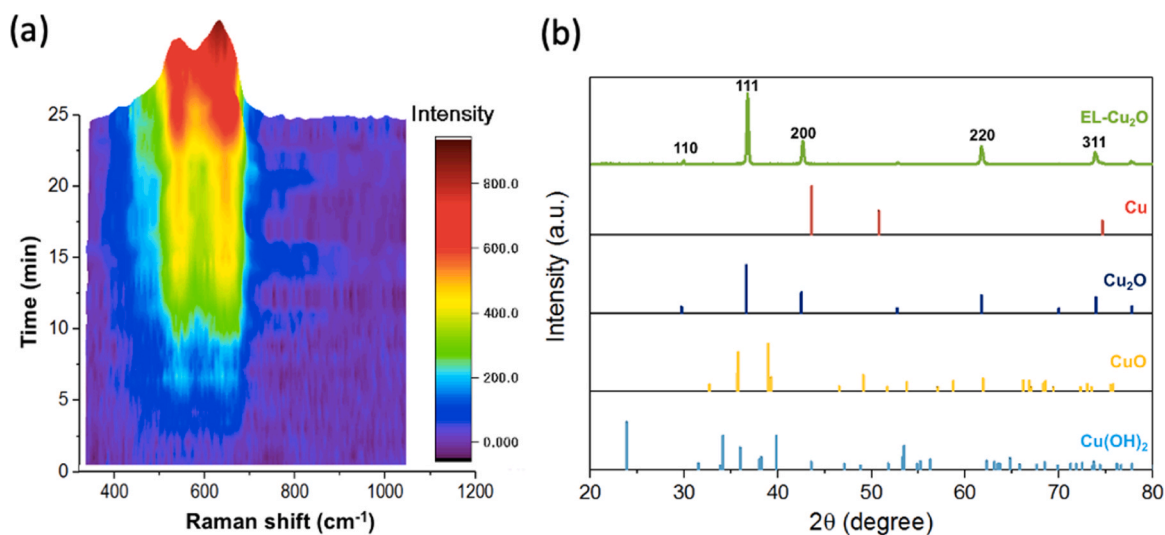
Fig. 5. (a) In situ Raman spectra of graphene/Cu foil in the CuSO$_4$ solution. (b) XRD pattern of the deposited particles.

optical and SEM images.

To clarify whether Cu$_2$O came from the corrosion of Cu foil or the reduction of Cu ions, the ICP-MS is employed to monitor the real-time concentration of Cu ion in CuSO$_4$ solution during electroless process. Meanwhile, the concentration of Cu ion could be calculated from the calibration curve (Fig. S5). It is found that the concentration of Cu ion in bath decreases with reaction time, demonstrating that the generated Cu$_2$O is attributed to the reduction of Cu ion (Fig. 6a). Besides, the amount of Cu ion is rapidly consumed within 6 h after the reaction, and then the amount gradually became constant. The amount of EL-Cu$_2$O is estimated through the consumed Cu ions, where almost no electroless plating occurred after 6 h, indicating the reaction was close to saturation. Additionally, the cross-section of SEM image via paraffin section shows the island-like Cu$_2$O generated on the partial surface of graphene within 1 h (Fig. 6b). The amount of island-like Cu$_2$O increases with the

reaction time (Fig. S6), and the island-like Cu$_2$O grows further and covers the surface of graphene nearly completely with the thickness of about 1.5 μm after 6 h. Besides, the SEM image illustrated the complete coverage of the graphene/Cu foil surface by electroless Cu$_2$O after electroless for 6 h (Fig. S7). At this point, the formed Cu$_2$O layer hinders the Cu ion to anchor on the defect sites of graphene, resulting in the stagnation of the electroless process which is consistent to the result of real-time ICP-MS. The EDS mapping of the cross-section of the growth sample clearly distinguish the deposited Cu$_2$O layer and metallic Cu foil (Fig. 6c).

To unravel the evolution process and growth site of Cu, the chemical state and local structure of EL-Cu$_2$O are probed by XAS along with Cu foil, Cu$_2$O and CuO reference spectra (Fig. 7a). According to the calibration standard obtaining from the maximum value of the first derivative of the X-ray absorption near-edge structure (XANES) of Cu foil (0),
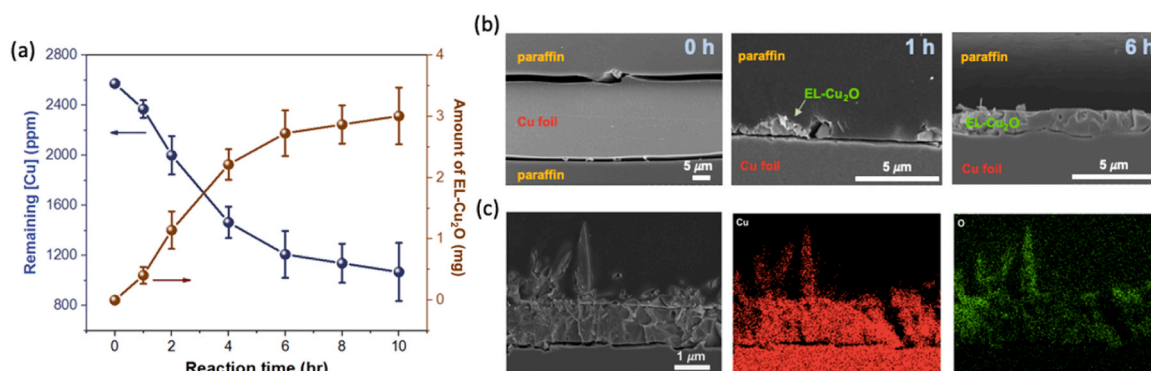
Fig. 6. (a) The concentration of remained Cu ion in the solution and the amount of deposited Cu on the sample. (b) The cross-sectional SEM images of graphene/Cu foil after 0, 1 and 6 h of reaction. (c) The cross-sectional EDS mapping of graphene/Cu foil after 6 h of reaction.
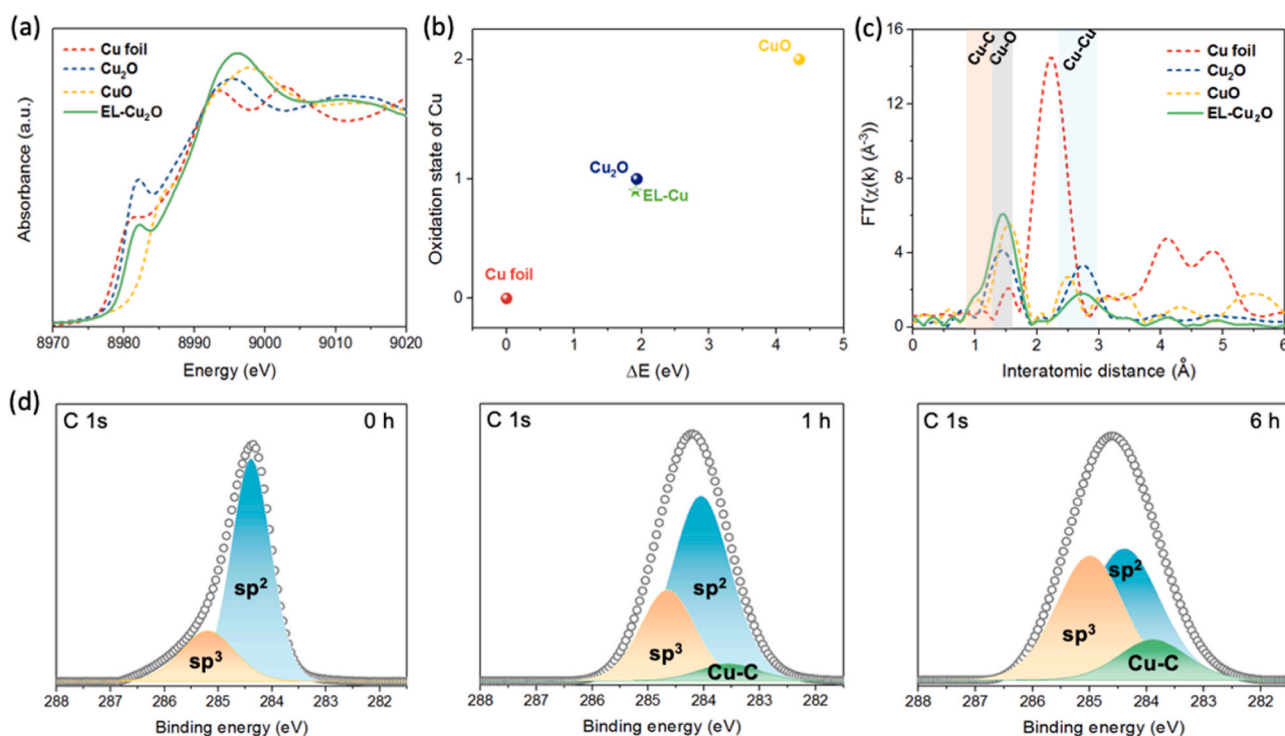
Fig. 7. (a) XANES spectra of Cu K-edge, (b) oxidation states of Cu and (c) EXAFS spectra of Cu K-edge. (d) C 1 s XPS of graphene/Cu foil after 0, 1 and 6 h of reaction.

Cu_2O (+1) and CuO (+2) (Fig. S8), the oxidation state of EL-Cu_2O was +0.89 (Fig. 7b). This result indicated EL-Cu representing a mixed valence system, involving Cu (1 +) and Cu (0), meaning that the most component of EL-Cu was Cu_2O with a small amount of metallic Cu. Therefore, it could be deduced that Cu^{2+} ions were initially reduced to metallic Cu before undergoing further oxidation in an aqueous solution to form Cu_2O, resulting in only a small amount of metallic Cu remaining. The Fourier-transformed k^3-weighted extended X-ray absorption fine structure (EXAFS) spectra of Cu K-edge of the EL-Cu shows a peak at R space of 1.5 Å and a peak at 2.7 Å bond, which were typically regarded as the Cu-O scattering path and secondary coordination shell of Cu-Cu, respectively (Fig. 7c) [39]. This R space is similar to that of Cu_2O standard sample, manifesting the structure of EL-Cu is Cu_2O. The EXAFS of EL-Cu also shows a small shoulder located at 1.1 Å, which is the Cu-C coordination [9].

Additionally, ex situ C 1 s XPS is used to examine the graphene structure in the duration of electroless process. The C 1 s XPS of pristine graphene on Cu foil can be deconvoluted into two peaks at 284.4 eV and 285.2 eV, which are assigned as sp^2 and sp^3 hybridization of carbon

bond (Fig. 7d) [40]. The defect carbon (sp^3 carbon bond) has already demonstrated by Raman spectrum (Fig. 1b). The new peak generated at 283.8 eV is observed after 1 h of electroless process, and this peak was assigned as Cu-C bond [41]. Evidence for Cu-C bonds in EXAFS and XPS suggested that the interface between EL-Cu and graphene was Cu-C bonds rather than Cu-O-C bonds as reported in the literatures [42,43]. This finding indicated that a strong connection is formed between EL-Cu_2O and graphene. Furthermore, the degrees of Cu-C bond and defect structure increase with the electroless time up to 6 h.

The in situ Raman spectra also reveal that the intensity ratio of D and G bands (I_D/I_G) increases with the electroless time, meaning that the in situ generation of defect structure occurred during electroless process (Fig. 8). In addition, some broad peaks are observed in the region between the G and D bands, and this can be attributed to the formation of amorphous carbon due to the increase of defects or disorders in the honeycomb structure of graphene [44]. It is worth mentioning that the formation of broad band located at 1755 cm^{-1} as observe during electroless is attributed to the CuC_4 structure [45,46], suggesting the initial growth site of CuC_4. Furthermore, the ratio of the D band to the G band
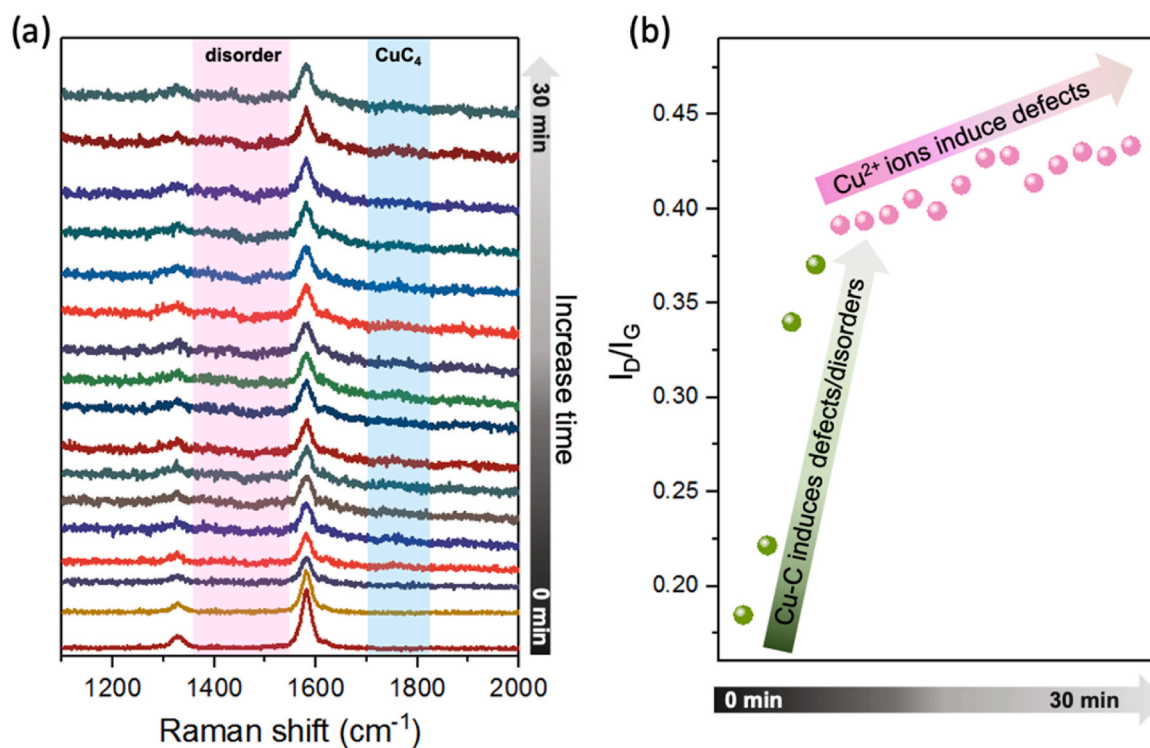
Fig. 8. (a) In situ Raman spectra of graphene/Cu foil in CuSO$_4$ solution. (b) The function of I$_D$/I$_G$ with reaction time.

exhibits two distinct behaviors over time (Fig. 8b). The combination of Cu^{2+} ions with the existing defect structures in graphene (formation of Cu-C) rapidly leads to the formation of amorphous carbon in the vicinity of defects. After this stage, most of the original defect structures had transformed into CuC$_4$ structures. Furthermore, Cu^{2+} ions induce the generation of defect structures, which predominantly governs the deposition rate and coverage completeness. This process occurs more slowly. Meanwhile, Cu^{2+} ions have a tendency to form coordination bonds with carbon atoms in graphene. In this case, the ligands are carbon atoms in graphene. The metal ions can bond to these carbon atoms through the sharing of electron pairs. The formation of coordination bonds between Cu^{2+} ions and carbon atoms can lead to the creation of defects in the graphene structure, including vacancies and disruptions in the regular hexagonal lattice. This phenomenon has also been mentioned in the literature [47].

To evaluate the adhesion between chemically deposited Cu$_2$O and graphene/Cu foil, the stability of the current values was assessed through electrochemical hydrogen evolution reactions. Fig. S9 displays the *i–t* chronoamperometric response of the Cu$_2$O nanoparticles-modified graphene/Cu foil (Cu$_2$O NPs/graphene/Cu foil) and electroless Cu$_2$O/graphene/Cu foil (EL-Cu$_2$O/graphene/Cu foil) at −1.2 V (vs RHE) in a 0.1 M KHCO$_3$ solution with saturated Ar. For Cu$_2$O NPs/graphene/Cu foil (Fig. S10), the preparation of suspended Cu$_2$O NPs followed a procedure in the literature, which involved the use of polyethylene glycol as a stabilizing agent and L-ascorbic acid as a reductant [28]. Additionally, a reaction time of 6 h for the electroless deposition of Cu$_2$O was chosen to ensure complete coverage of the graphene/Cu foil surface by Cu$_2$O. Over time, the catalytic current of Cu$_2$O NPs/graphene/Cu foil without Nafion decreased, suggesting that Cu$_2$O NPs detachment reduced the active site population during electrochemical hydrogen evolution. In contrast, the electrocatalytic current density of EL-Cu$_2$O/graphene/Cu foil remains stable, suggesting a strong interaction between either the deposited Cu$_2$O and Cu$_2$O or Cu$_2$O and graphene/Cu foil.

To evaluated the impact of the proposed electroless Cu$_2$O deposition method on surface roughness using electrochemically active surface area (ECSA). ECSA is typically directly correlated with the roughness of the electrode surface. In electrochemistry, the surface roughness of an electrode increases the available surface area, leading to a greater number of active sites on the electrode. Therefore, a larger rough surface area generally implies a larger ECSA. The ECSA values for graphene/Cu foil, EL-Cu$_2$O/graphene/Cu foil and Cu$_2$O NPs/graphene/Cu foil can be determined by extracting the double-layer capacitance (C$_{dl}$) through cyclic voltammetry (CV) measurements in the non-Faradaic potential region. Subsequently, ECSA is calculated using the equation: ECSA = C$_{dl}$/C$_s$, where C$_s$ represents the specific capacitance of the electrocatalysts. The value of C$_{dl}$ can be obtained through plotting the average difference between forward and reverse currents at the middle of the potential window against scan rates (Fig. S11). Furthermore, ECSA values can be calculated by dividing C$_{dl}$ by a specific capacitance of 40 μF cm^{-2}, typical for transition-metal oxides. Therefore, at a fixed geometric area of 1 cm^{-2}, the ECSA values for graphene/Cu foil, EL-Cu$_2$O/graphene/Cu foil and Cu$_2$O NPs/graphene/Cu foil are 20.0, 52.5, and 70.0 cm^2, respectively. Additionally, the roughness factor, which represents the ratio of the real surface area to the geometric surface area, can be determined by dividing the ECSA by the geometric electrode area (1 cm^{-2}). The roughness factors for graphene/Cu foil, EL-Cu$_2$O/graphene/Cu foil and Cu$_2$O NPs/graphene/Cu foil are 20.0, 52.5 and 70.0, respectively. These results indicate that the surface of graphene/Cu foil exhibited some degree of roughness, as observed in surface morphology of SEM (Fig. S2a). In comparison, the EL-Cu$_2$O/graphene/Cu foil results in a lower surface roughness compared to Cu$_2$O NPs/graphene/Cu foil.

The growth sites of Cu and the mechanism of electroless process is proposed based on aforementioned results. As shown in Fig. 9, the defect site of graphene on slightly oxidized Cu foil provided an anchor site for Cu ion via Cu-C bonding to stabilize Cu ion. The anchored Cu of CuC$_4$ was one type of Cu single-atom structure, which was considered as the electron reservoir and highly active. Under irradiation, the photoelectrons generated from the thin Cu$_2$O layer at the interface of graphene and Cu foil were accumulated on the anchored Cu site. This electron-rich site then reduced the Cu ions to metallic Cu particles. In addition to the defect structure, the adsorption energy of Cu to the sp^2 carbon structure
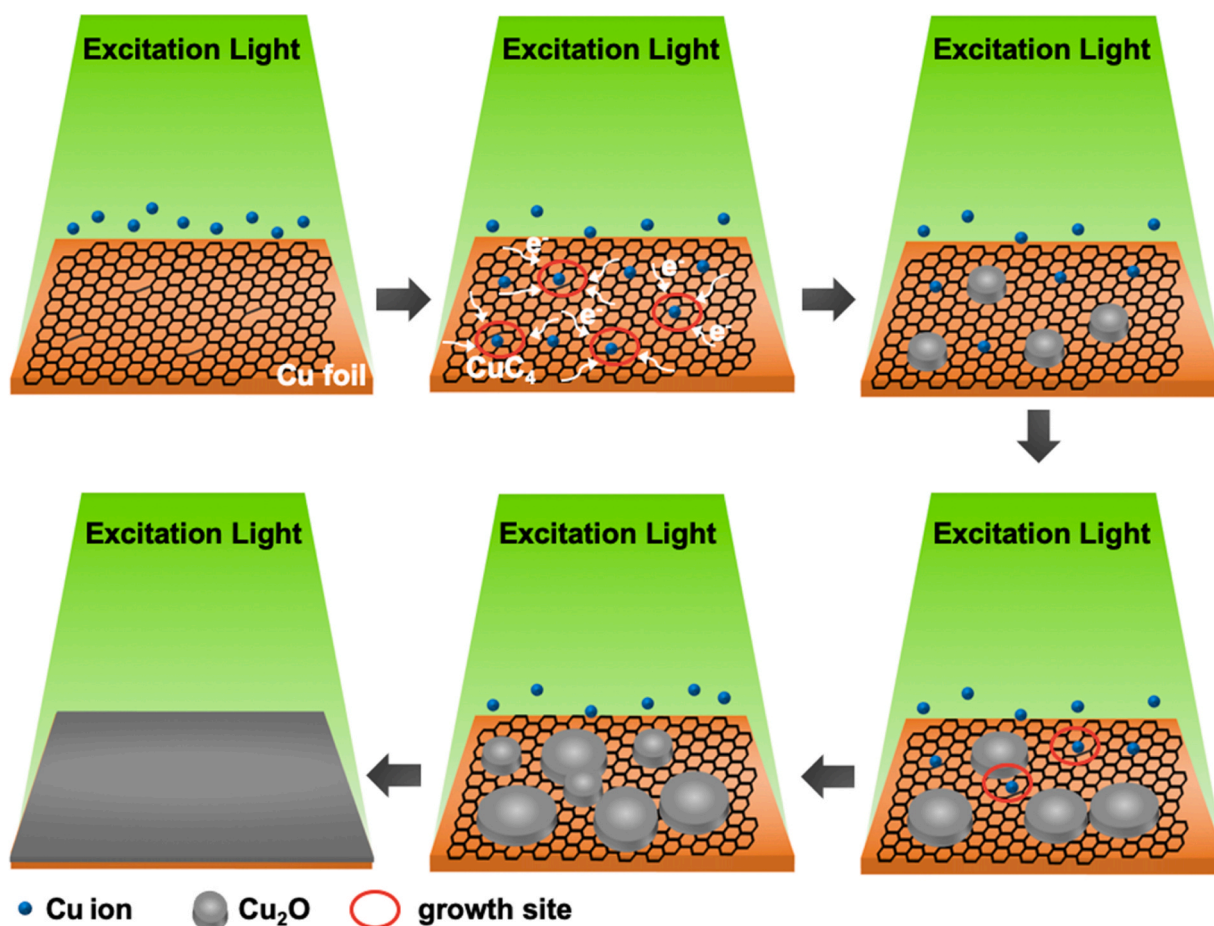
Fig. 9. Schematic of the electroless process of Cu_2O on graphene/Cu_2O/Cu foil. (the red circles represent the formation of CuC_4 structure through trapping Cu ions on defect structure of graphene.).

was lower than the cohesive energy of Cu species, resulting in the island-like growth of Cu through Cu-Cu interaction in the initial state [47–49]. Subsequently, most of the reduced Cu was instantaneously oxidized to Cu_2O due to the lack of a strong reducing agent. Therefore, only a small amount of metallic Cu was observed by XAS. At the same time, the interaction of Cu ion to graphene could damage the sp^2 bonding network of graphene [39], creating more defect sites for further deposition of Cu until the graphene surface was covered by Cu_2O completely.

To further demonstrate the practicability of this green electroless process, different metal ion solutions were used on graphene/Cu foil for 6 h under green light irradiation. As shown in Fig. S12, zinc, titanium, cobalt, cerium or cadmium ions can all be deposited on the graphene/Cu foil, respectively. Among them, the deposited cobalt oxide showed the lowest dispersion density. This phenomenon can be attributed to the non-photoelectric property of cobalt oxide which could not provide the extra photoexcited electrons to promote epitaxial growth. In contrast,
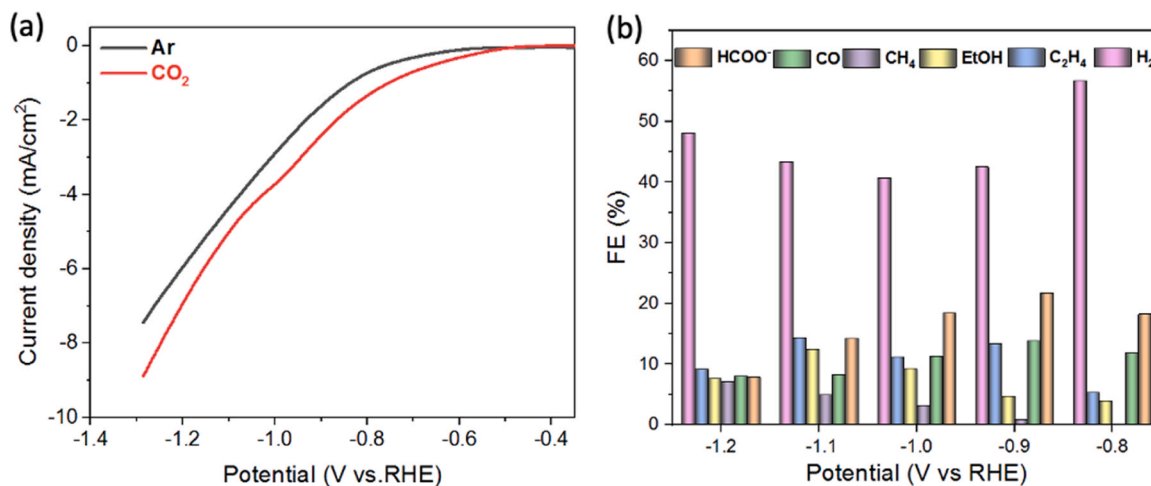
Fig. 10. CO_2RR activity of EL-Cu_2O in 0.1 M $KHCO_3$. (a) LSV curves of EL-Cu_2O/graphene/Cu foil with the scan rate of 10 mV/s. (b) FEs of each product at constant potential.

the photoelectric properties of zinc oxide, titanium oxide, cerium oxide and cadmium oxide lead to high dispersion densities. Surprisingly, the deposition of gold and silver covered the entire surface within 10 min, which was notably faster than the deposition time of other metals. Furthermore, SEM-EDS analysis indicated that no oxides were formed, suggesting that species like metallic Au and Ag, which are not prone to oxidation, remain in their metallic state under this electroless deposition process.

Moreover, to ascertain whether EL-Cu_2O exhibits characteristics suitable for electrochemical CO_2RR, we performed linear sweep voltammetry (LSV) on EL-Cu_2O/graphene/Cu foil in two different electrolytes: one saturated with Ar and the other saturated with CO_2, both of which were in a 0.1 M $KHCO_3$ solution were performed. As depicted in Fig. 10a, the electrochemical behavior in the electrolyte saturated with CO_2 displayed distinct differences compared to that saturated with Ar, indicating the activity of Cu_2O/graphene/Cu foil in electrochemical CO_2RR. To investigate the relationship between potential and product formation, experiments on CO_2RR were conducted using a customized H-type cell comprising two gastight compartments separated by an anion-exchange membrane. Meanwhile, chronoamperometry was carried out to analyze product distribution at various applied potentials. Fig. 10b illustrated the faradaic efficiency (FE) of the products as a function of the applied potential. In addition to hydrogen evolution, the main products at low reduction potentials were formate and CO. This outcome was attributed to the electroreduction of the of CO_2 molecules through the O atom- and C atom-coordinated to Cu, respectively. As the potential increased, the probability of *CO and *CO coupling increases, leading to higher FEs of C_{2+} products (C_2H_5OH and C_2H_4). At higher potentials, CH_4 becomes the predominant product. The product profile confirmed the electrocatalytic behavior of EL-Cu_2O in the CO_2RR.

3. Conclusion

In summary, a graphene-assisted approach of triggering metal deposition under irradiation develops a truly environmentally friendly process. According to the evidences of ex situ XAS, XPS and in situ Raman spectroscopy, the mechanism of electroless deposition is proposed. The in situ generation of graphene defect structure can contribute more growth sites, resulting in deposited metal/metal oxide particles with high dispersion density on graphene surface. Additionally, the formation of Cu-C bond at the interface reinforces the interaction between deposited Cu and graphene layer, avoiding the separation in the working state. The prepared Cu_2O/graphene/Cu structure can be used as oxide-derived Cu electrocatalyst in electrochemical CO_2 reduction reaction.

4. Experimental

4.1. Deposition of Cu on graphene/Cu foil

Monolayer graphene on Cu foil (graphene/Cu foil) was purchased from Graphenea Inc. The graphene/Cu foil with an exposed area of 1 cm^2 was designed for immersion in 5 mM $CuSO_4$ solution at a stirring rate of 200 rpm. The reaction cell was irradiated by blue, green, red and white LEDs with the wavelength of 463, 524, 632 and 452 coupling 547 nm, respectively. After irradiation with different times, the impregnated graphene/Cu foil samples were washed with DI water and dried in vacuum oven.

4.2. Structural characterization

Field emission scanning electron microscopy (FE-SEM) images were obtained with Hitachi SU8220, and Energy-dispersive X-ray spectroscopy (EDX) mapping was conducted by HORIBA X-max. The crystalline structure analysis was studied by X-ray diffraction (XRD, Bruker D2 Phaser) using Cu Kα radiation (λ = 1.54 Å). The XPS analysis was done with a PHI 5000 Versa Probe (ULVAC-PHI, Japan) system, using a monochromatic Al Kα X-ray. The XAS of Cu K-edge were obtained at SPring-8 (Japan) 12B2 Taiwan beamline of the National Synchrotron Radiation Research Center (NSRRC) operated at 8.0 GeV with a constant current of ~100 mA. In situ Raman spectroscopy was performed by UniDRON (CL Technology) with a 50 × objective lens and a 633 nm laser. XPS spectra were acquired using a PHI 5000 VersaProbe (ULVAC-PHI, Japan) system. During the measurement, a monochromatic Al Kα X-ray with a beam diameter of 100 μm was used.

4.3. Atomic scale modelling and simulation methodology

To have a better understanding of the effects of defect sites of single layer graphene, atomic scale modeling is employed. A pure Fm-3 m face centered cubic structure of Cu was used for the calculation where the system consisted of 80 atoms. Above the pure Cu 18 molecules of Cu_2O was layered which represented miniscule oxidations occurring from Oxygen present in the storage before graphene layering. A graphene sheet containing single and double defect sites was introduced over the Cu-Cu_2O system. The density functional theory (DFT) calculations are carried out by projector-augmented wave (PAW) method as implemented in the Vienna Ab-initio Simulation Package provided by Medea (Medea-VASP). The interactions are described using the Generalized Gradient Approximation with Perdew-Burke-Ernzerhof (GGA-PBE) exchange-correlation functional. The atomic orbitals are defined by plane-wave basis sets with cut-off energies of 396.0 eV. Real space projection operators are used and the convergence criterion for self-consistent field calculations is set to 10^{-5} eV between consecutive steps. The convergence criterion for atomic forces of the systems is set to be less than 0.002 eV A^{-1}. The Brillouin zone is sampled at 4 × 4 × 4 gamma centered k-points where the actual k-point spacing is $0.079 \times 0.063 \times 0.052$ per Angstrom. The structures were optimized after stacking of each layer, while formation of the system to observe the interactions between each molecular species.

CRediT authorship contribution statement

Chen Hsiao-Chien: Conceptualization, Data curation, Methodology, Supervision, Writing – original draft, Writing – review & editing. **Shabir Abdul:** Methodology, Writing – original draft. **Tu Kun-Hua:** Methodology, Validation. **Tan Cher Ming:** Conceptualization, Supervision, Writing – review & editing. **Chiu Wei-Hao:** Methodology, Validation. **Fan Ruei-Cheng:** Methodology, Validation. **Baruah Nilim Akash:** Visualization.

Declaration of Competing Interest

The authors declare the following financial interests/personal relationships which may be considered as potential competing interests: Hsiao-Chien Chen reports financial support was provided by National Science and Technology Council.

Data availability

Data will be made available on request.

Acknowledgements

Appendix A. Supporting information

Supplementary data associated with this article can be found in the online version at doi:10.1016/j.jece.2023.111741.

References

[1] Y. Yu, H. Wang, J. Hu, Co-treatment of electroplating sludge, copper slag, and spent cathode carbon for recovering and solidifying heavy metals, J. Hazard. Mater. 417 (2021), 126020.

[2] S. Zhang, F. Zhang, Z. Zhang, G. Li, H. Fu, J. Huang, Y. Wang, An electroless nickel plating fabric coated with photothermal Chinese ink for powerful passive anti-icing/icephobic and fast active deicing, Chem. Eng. J. 450 (2022), 138328.

[3] Z. Wang, Y. Wu, B. Zhu, Q. Chen, Y. Zhang, Z. Xu, D. Sun, L. Lin, D. Wu, Self-patterning of highly stretchable and electrically conductive liquid metal conductors by direct-write super-hydrophilic laser-induced graphene and electroless copper plating, ACS Appl. Mater. Interfaces 3 (2023) 4713–472325.

[4] H. Rong, C. Zhang, Y. Sun, L. Wu, B. Lian, Y. Wang, Y. Chen, Y. Tu, T.D. Waite, Electrochemical degradation of Ni-EDTA complexes in electroless plating wastewater using PbO2-Bi electrodes, Chem. Eng. J. 431 (2022), 133230.

[5] L. Qu, L. Dai, E. Osawa, Shape/size-controlled syntheses of metal nanoparticles for site-selective modification of carbon nanotubes, J. Am. Chem. Soc. 16 (2006) 5523–5532.

[6] Y. Bian, H. Wang, Z. Gao, J. Hu, D. Liu, L. Dai A facile approach to high-performance trifunctional electrocatalysts by substrate-enhanced electroless deposition of Pt/NiO/Ni on carbon nanotubes. Nanoscale. 12 (2020), pp. 14615–14625.

[7] Y. Tang, Z. Yang, X. Dai, Trapping of metal atoms in the defects on graphene, J. Chem. Phys. 135 (2011), 224704.

[8] Y. Jia, L. Zhang, A. Du, G. Gao, J. Chen, X. Yan, C.L. Brown, X. Yao, Defect graphene as a trifunctional catalyst for electrochemical reactions, Adv. Mater. 28 (2016) 9532–9538.

[9] L. Zhang, Y. Jia, G. Gao, X. Yan, N. Chen, J. Chen, M.T. Soo, B. Wood, D. Yang, A. Du, X. Yao, Graphene defects trap atomic Ni species for hydrogen and oxygen evolution reactions, Chem 4 (2018) 285–297.

[10] Q. Cheng, C. Hu, G. Wang, Z. Zou, H. Yang, L. Dai, Carbon-defect-driven electroless deposition of Pt atomic clusters for highly efficient hydrogen evolution, J. Am. Chem. Soc. 142 (2020) 5594–5601.

[11] J. Zhang, Y. Deng, X. Cai, Y. Chen, M. Peng, Z. Jia, Z. Jiang, P. Ren, S. Yao, J. Xie, D. Xiao, X. Wen, Tin-assisted fully exposed platinum clusters stabilized on defect-rich graphene for dehydrogenation reaction, ACS Catal. 7 (2019) 5998–60055.

[12] Z. Chen, J. Zhang, S. Deng, M. Hou, X. Zhang, Z. Jiang, N.C. Lai, Morphology-controlled synthesis of Cu2O encapsulated phase change materials: photothermal conversion and storage performance in visible light regime, Chem. Eng. J. 454 (2023), 140089.

[13] S. Luo, R. Liu, X. Zhang, R. Chen, M. Yan, K. Huang, J. Sun, R. Wang. Mechanism investigation for ultra-efficient photocatalytic water disinfection based on rational design of indirect Z-scheme heterojunction black phosphorus QDs/Cu2O nanoparticles. J. Hazard. Mater. 424 (2022), p. 127281.

[14] J. Wang, H.C. Chen, H.Y. Tan, C.M. Tan, Y. Zhu, H.M. Chen, Strong correlation between the dynamic chemical state and product profile of carbon dioxide electroreduction, ACS Appl. Mater. Interfaces 20 (2022) 22681–22696.

[15] D.H. Wi, H. Yang, Y. Kim, H. Ahn, J.W. Hong, Metal-semiconductor-metal ternary heteronanocrystals with multiple plasmonic effects for efficient photocatalysis, J. Mater. Chem. A 11 (2022) 1343–1350.

[16] J. Zhou, F. Pan, Q. Yao, Y. Zhu, Achieving efficient and stable electrochemical nitrate removal by in-situ reconstruction of Cu2O/Cu electroactive nanocatalysts on Cu foam, Appl. Catal. B 317 (2022), 121811.

[17] D. Li, T. Liu, L. Huang, J. Wu, J. Li, L. Zhen, Y. Feng, Selective CO2-to-formate electrochemical conversion with core-shell structured Cu2O/Cu@C composites immobilized on nitrogen-doped graphene sheets, J. Mater. Chem. A 35 (2020) 18302–18309.

[18] J.Y. Kim, G. Kim, H. Won, I. Gereige, W.B. Jung, Synergistic effect of Cu2O mesh pattern on high-facet Cu surface for selective CO2 electroreduction to ethanol, Adv. Mater. 3 (2022) 2106028.

[19] Y. Wang, H. Lei, S. Lu, Z. Yang, B.B. Xu, L. Xing, T.X. Liu, Cu2O nano-flowers/graphene enabled scaffolding structure catalyst layer for enhanced CO2 electrochemical reduction, Appl. Catal. B 305 (2022), 121022.

[20] C.J. Chang, S.F. Hung, C.S. Hsu, H.C. Chen, S.C. Lin, Y.F. Liao, H.M. Chen, Quantitatively unraveling the redox shuttle of spontaneous oxidation/electroreduction of CuOx on silver nanowires using in situ X-ray absorption spectroscopy, ACS Cent. Sci. 5 (2019) 1998–2009.

[21] H. Jung, S.Y. Lee, C.W. Lee, M.K. Cho, D.H. Won, C. Kim, H.S. Oh, B.K. Min, Y. J. Hwang, Electrochemical fragmentation of Cu2O nanoparticles enhancing selective C–C coupling from CO2 reduction reaction, J. Am. Chem. Soc. 141 (2019) 4624–4633.

[22] Y.E. Kim, W. Lee, Y.N. Ko, J.E. Park, D. Tan, J. Hong, Y.E. Jeon, J. Oh, K. T. Park. Role of binder in Cu2O gas diffusion electrodes for CO2 reduction to C2+ products, ACS Sustain. Chem. Eng. 36 (2022) 11710–11718.

[23] M. Mallik, S. Monia, M. Gupta, A. Ghosh, M.P. Toppo, H. R Synthesis and characterization of Cu2O nanoparticles. J. Alloys Compd. 829 (2020), p. 154623.

[24] M. Debbarma, P. Sutradhar, M. Saha, Synthesis of Cu2O nanoparticles and current–voltage measurements (I-V) of its nanocomposites, Nanotechnol. Environ. Eng. 1 (2016), 6.

[25] L. Xiong, S. Xiao, S. Chen, Z. Chen, X. Yi, S. Wen, G. Zheng, Y. Ding, H. Yu, Fast and simplified synthesis of cuprous oxide nanoparticles: annealing studies and photocatalytic activity, RSC Adv. 4 (2014) 62115–62122.

[26] M.H. Kim, B. Lim, E.P. Lee, Y. Xia. Polyol synthesis of Cu2O nanoparticles: use of chloride to promote the formation of a cubic morphology. J. Mater. Chem. 18 (2008), pp. 4069–4073.

[27] Y.E. Kim, J.E. Park, J.H. Lee, H. Choi, W. Lee, Y.N. Ko, H.Y. Kim, K.T. Park, Ag decorated-Cu2O catalysts with enhanced selectivity for CO2 electroreduction toward C2+ products, J. Environ. Chem. Eng. 11 (2023), 111028.

[28] D. Hong, G. Cao, J. Qu, Y. Deng, J. Tang, Antibacterial activity of Cu2O and Ag co-modified rice grains-like ZnO nanocomposites, J. Mater. Sci. Technol. 34 (2018) 2359–2367.

[29] V. Soni, Sonu, P. Singh, S. Thakur, P. Thakur, T. Ahamad, V.H. Nguyen, Q.V. Le, C. M. Hussain, P. Raizada, Fabricating cattle dung-derived nitrogen-doped biochar supported oxygen-deficient ZnO and Cu2O-based novel step-scheme photocatalytic system for aqueous Doxycycline hydrochloride mitigation and Cr (VI) reduction, J. Environ. Chem. Eng. 11 (2023), 110856.

[30] Y.P. Huang, C.W. Tung, T.L. Chen, C.S. Hsu, M.Y. Liao, H.C. Chen, H.M. Chen, In situ probing the dynamic reconstruction of copper-zinc electrocatalyst for CO2 reduction, Nanoscale 14 (2022) 8944–8950.

[31] C.J. Chang, S.C. Lin, H.C. Chen, J. Wang, K.J. Zheng, Y. Zhu, H.M. Chen, Dynamic reoxidation/reduction-driven atomic interdiffusion for highly selective CO2 reduction toward methane, J. Am. Chem. Soc. 28 (2020) 12119–12132.

[32] Z. Zhao, T. Hou, N. Wu, S. Jiao, K. Zhou, J. Yin, J.W. Suk, X. Cui, M. Zhang, S. Li, Y. Qu, W. Xie, X.B. Li, C. Zhao, Y. Fu, R.D. Hong, S. Guo, D. Lin, W. Cai, W. Mai, Z. Luo, Y. Tian, Y. Lai, Y. Liu, L. Colombo, Y. Hao, Polycrystalline few-layer graphene as a durable anticorrosion film for copper, Nano Lett. 2 (2021) 1161–1168.

[33] A. Chakravarty, K. Bhowmik, A. Mukherjee, G. De, Cu2O nanoparticles anchored on amine-functionalized graphite nanosheet: a potential reusable catalyst, Langmuir 18 (2015) 5210–5219.

[34] Q. Hu, Z. Han, X. Wang, G. Li, Z. Wang, X. Huang, H. Yang, X. Ren, Q. Zhang, J. Liu, Prof C. He, Facile synthesis of sub-nanometric copper clusters by double confinement enables selective reduction of carbon dioxide to methane, Angew. Chem. Int. Ed. 59 (2020) 19054–19059.

[35] W. Gao, J.E. Mueller, Jo Anton, Q. Jiang, T. Jacob, Nickel cluster growth on defect sites of graphene: a computational study, Angew. Chem. Int. Ed. 52 (2013) 14237–14241.

[36] K. Shimura, H. Yoshida, Heterogeneous photocatalytic hydrogen production from water and biomass derivatives, Energy Environ. Sci. 4 (2011) 2467–2481.

[37] N.A. Saad, M.H. Dar, E. Ramya, S.R.G. Naraharisetty, D.N. Rao, J. Mater. Sci. 54 (2019) 188–199.

[38] K.P. Ganesan, N. Anandhan, A. Amaliroselin, R. Thangamuthu, T. Marimuthu, R. Panneerselvam, J. Mater. Sci. Mater. Electron. 30 (2019) 15482–15492.

[39] C.J. Chang, Y. Zhu, J. Wang, H.C. Chen, C.W. Tung, Y.C. Chu, H.M. Chen, In situ X-ray diffraction and X-ray absorption spectroscopy of electrocatalysis for energy conversion reactions, J. Mater. Chem. A 8 (2020) 19079–19112.

[40] L.L. Dong, W.G. Chen, N. Deng, C.H. Zheng, A novel fabrication of graphene by chemical reaction with a green reductant, Chem. Eng. J. 306 (2016) 754–762.

[41] F. Huang, Y. Deng, Y. Chen, X. Cai, M. Peng, Z. Jia, J. Xie, D. Xiao, X. Wen, N. Wang, Z. Jiang, H. Liu, D. Ma, Anchoring Cu species over nanodiamond-graphene for semi-hydrogenation of acetylene, Nat. Commun. 10 (2019) 4431.

[42] P.H. Manrique, X. Lei, R. Xu, M. Zhou, I.A. Kinloch, R.J. Young, Copper/graphene composites: a review, J. Mater. Sci. 54 (2019) 12236–12289.

[43] X. Zhang, C. Shi, E. Liu, N. Zhao, C. He, Effect of interface structure on the mechanical properties of graphene nanosheets reinforced copper matrix composites, ACS Appl. Mater. Interfaces 10 (2018) 37586–37601.

[44] S.K. Sengar, B.R. Mehta, R. Kumar, V. Singh, In-flight gas phase growth of metal/multi layer graphene core shell nanoparticles with controllable sizes, Sci. Rep. 3 (2013) 2814.

[45] H. Li, S.L. Liu, Z. Xie, C. Bai, Copper-carbon clusters CunCm (n, m = 1–6): segregation, bonding and raman spectra, Mater. Today Commun. 26 (2021), 102035.

[46] Y. Jia, T. Zhang, M. Liu, J. Zhang, Y. Han, Effect of different heteroatoms anchoring a Cu single-atom catalyst on acetylene hydrochlorination, J. Phys. Chem. C 126 (48) (2022) 20401–20410.

[47] I.A. Pašti, A. Jovanović, A.S. Dobrota, S.V. Mentus, B. Johansson, N. V. Skorodumova, Atomic adsorption on pristine graphene along the periodic table of elements – from PBE to non-local functionals, Appl. Surf. Sci. 436 (2018) 433–440.

[48] I.A. Pašti, A. Jovanović, A.S. Dobrota, S.V. Mentus, B. Johansson, N. V. Skorodumova, Atomic adsorption on graphene with a single vacancy: systematic DFT study through the periodic table of elements, Phys. Chem. Chem. Phys. 20 (2018) 858–865.

[49] L.D. Rafailović, A.Z. Jovanović, S.J. Gutić, J. Wehr, C. Rentenberger, T.Lj Trišović, I.A. Pašti, New insights into the metallization of graphene-supported composite materials-from 3D Cu-Grown structures to free-standing electrodeposited porous Ni foils, ACS Omega 5 (2022) 4352–4362.